

# A highly dispersed and anti-coking Ni–La<sub>2</sub>O<sub>3</sub>/SiO<sub>2</sub> catalyst for syngas production from dry carbon dioxide reforming of methane†

Cite this: *Catal. Sci. Technol.*, 2014, 4, 2107

Liuye Mo, Kerina Kai Mun Leong and Sibudjing Kawi\*

Received 31st October 2013,  
Accepted 23rd March 2014

DOI: 10.1039/c3cy00869j

www.rsc.org/catalysis

Syngas production from dry carbon dioxide reforming of methane was studied on a Ni/SiO<sub>2</sub> doped with La<sub>2</sub>O<sub>3</sub> catalyst prepared *via* an *in situ* self-assembled core-shell precursor route. Highly dispersed nickel of particle size <3.0 nm on the Ni–La<sub>2</sub>O<sub>3</sub>/SiO<sub>2</sub> catalyst was successfully achieved. The addition of La<sub>2</sub>O<sub>3</sub> enhanced the interaction between NiO and the silica support to form a more stable nickel silicate. The resulting Ni–La<sub>2</sub>O<sub>3</sub>/SiO<sub>2</sub> catalyst showed excellent catalytic activity and stability without any coking behaviour even after 100 hours of reaction on stream. In contrast, the Ni–La<sub>2</sub>O<sub>3</sub>/SiO<sub>2</sub> catalyst prepared using a conventional incipient wetness impregnation method exhibited poor catalytic activity and a high coke formation rate.

## Introduction

Dry carbon dioxide reforming of methane (DRM: CO<sub>2</sub> + CH<sub>4</sub> → 2CO + 2H<sub>2</sub>) to produce syngas (CO/H<sub>2</sub>) has garnered increasing interest due to its potential for the reduction of emission of greenhouse gases carbon dioxide (CO<sub>2</sub>) and methane (CH<sub>4</sub>).<sup>1</sup> The syngas from DRM can be used as a feedstock for many petrochemical processes, *e.g.* synthesis of methanol and ammonia and, more importantly, Fischer–Tropsch synthesis of liquid hydrocarbons. The advantage of the conversion of syngas to liquid hydrocarbons is that liquid hydrocarbons are easier and less costly to transport compared to gaseous fuel.<sup>1</sup> There are great economic and environmental incentives to convert CH<sub>4</sub> to syngas *via* DRM, but it has not yet been adapted for large-scale industrial applications. The main problem that plagues DRM is the presence of severe carbon formation, which may block the catalyst beds and deactivate the catalysts.<sup>2,3</sup> Hence, in the design of catalysts for dry reforming of CH<sub>4</sub>, carbon deposition is the principal difficulty that must be overcome.

Noble metal catalysts such as Rh, Ru and Ir have been found to exhibit high activity and stability for DRM. More importantly, they exhibit good resistance to carbon deposits.<sup>4–6</sup> The drawback in using noble metals is that they are limited in resources and are expensive.<sup>7</sup> Therefore, utilization of cheaper and more abundant non-noble metal catalysts, particularly

Ni-based catalysts, is more attractive.<sup>8</sup> DRM reaction using Ni catalysts has been found to be comparable to that using noble metal catalysts.<sup>9</sup>

The catalyst support utilized will also have a big role to play in the performance of the catalyst. Wang and Lu reported that carbon deposition would be more significant if there were weaker interactions between the active metal and the support and that a catalyst with “well-developed porosity” would exhibit better catalytic activity. In their research, SiO<sub>2</sub>, Al<sub>2</sub>O<sub>3</sub> and MgO were used as supports for Ni-based catalysts and they concluded that Ni/γ-Al<sub>2</sub>O<sub>3</sub> and Ni/MgO catalysts prepared using commercial MgO achieve high conversion and long-term stability but not the Ni/SiO<sub>2</sub> catalyst.<sup>10</sup> Wang and Ruckenstein also concluded that γ-Al<sub>2</sub>O<sub>3</sub> and MgO supports show the greatest potential in producing good catalysts for CH<sub>4</sub> dry reforming reaction in terms of high activity, long-term stability and CO/H<sub>2</sub> yield.<sup>11</sup> La<sub>2</sub>O<sub>3</sub>, which has moderate basicity to adsorb and form La<sub>2</sub>O<sub>2</sub>CO<sub>3</sub> during reaction, is a good nickel catalyst support for DRM.<sup>12,13</sup> Our previous studies showed that high catalytic activity on the SrO-doped Ni/La<sub>2</sub>O<sub>3</sub> catalyst is attributed to the presence of a high amount of lattice oxygen surface species which promotes C–H activation in DRM reaction, resulting in high H<sub>2</sub> production.<sup>14</sup> Lately, we also found that nickel supported on LaAlO<sub>3</sub>–Al<sub>2</sub>O<sub>3</sub> would form inverse NiAl<sub>2</sub>O<sub>4</sub> spinel, which exhibits unique catalytic characteristics for DRM.<sup>15</sup> Boron oxide can also be used to improve the Ni/Al<sub>2</sub>O<sub>3</sub> catalyst's activity and stability by producing an O–H group, which can significantly facilitate carbon removal and improve the stability of the catalysts.<sup>16</sup> Furthermore, nickel supported on ZrO<sub>2</sub> with particle sizes ranging from 10–15 nm formed a nanocomposite which displayed excellent activity and

Department of Chemical and Biomolecular Engineering, National University of Singapore, Singapore 117576. E-mail: chekawis@nus.edu.sg;

Fax: +(65) 6779 1936; Tel: +(65) 6516 6312

† Electronic supplementary information (ESI) available: XRD and DTA-TGA results. See DOI: 10.1039/c3cy00869j

stability.<sup>17</sup> Zheng's group developed a catalyst of nickel supported on MgAl<sub>2</sub>O<sub>4</sub> spinel, which showed high activity and carbon resistance toward DRM, attributed to high nickel dispersion and the strong interaction between nickel and the support.<sup>18</sup> In support of the above results, our recent findings revealed that magnesium oxide, besides enhancing the basicity of the catalyst, also created surface oxygen ion species, stabilized the monoclinic La<sub>2</sub>O<sub>2</sub>CO<sub>3</sub> crystal phase, which is able to oxidize and remove deposited carbon, and kept the Ni catalyst highly active and stable.<sup>19</sup>

The nickel catalysts derived from solid solution catalysts or complex oxides are also attractive catalysts as highly dispersed metal nickel can be achieved after reduction. Tomishige<sup>20,21</sup> and Hu<sup>22</sup> found that nickel–magnesium oxide catalysts from the reduced nickel oxide–magnesium oxide solid solution catalyst resulted in high dispersion of reduced Ni species, basicity of the support surface and nickel–support interaction. The catalytic activity and stability of the nickel oxide–magnesium oxide solid solution could be further improved by addition of a small amount of a noble metal, which promotes the reducibility of nickel oxide, forming a nickel–noble metal alloy.<sup>23,24</sup> Zhang reported stable and high catalytic activities of nickel–cobalt bimetallic catalysts from Ni–Co–Al–Mg–O composites.<sup>25</sup> The high activity and excellent stability of Ni–Co catalysts are closely related to the high metal dispersion, strong metal–support interaction, and formation of stable solid solutions. Nickel catalysts prepared from perovskite precursors have also been used for DRM.<sup>26–28</sup> Our group reported that La<sub>0.8</sub>Sr<sub>0.2</sub>Ni<sub>0.8</sub>Fe<sub>0.2</sub>O<sub>3</sub> shows high catalytic stability due to: (1) strong metal–support interaction which hinders thermal agglomeration of the Ni particles and (2) the presence of the abundant lattice oxygen species which are not very active for C–H bond activation but reactive with CO<sub>2</sub> forming La<sub>2</sub>O<sub>2</sub>CO<sub>3</sub>, which minimizes carbon formation by reacting with surface carbon to form CO.<sup>29</sup>

Although SiO<sub>2</sub> is cheap and easily available, the main drawback in using SiO<sub>2</sub> as the support for Ni-based catalysts is its high tendency towards carbon deposition and metal sintering.<sup>30–34</sup> The poor performance of SiO<sub>2</sub> as the catalyst support for dry reforming of CH<sub>4</sub> has been attributed to weak interactions between Ni and the SiO<sub>2</sub> support and its inability to promote high dispersion of Ni particles on the support surface.<sup>33</sup> In addition, with weak interactions between Ni and the SiO<sub>2</sub> support, Ni metal particles are more likely to move along the support surface and agglomerate during heating at high temperatures, resulting in comparatively larger Ni particle sizes and metal sintering during reaction. However, siliceous based materials such as supports of nickel and nickel–M bimetallic catalysts, especially mesoporous materials (like MCM-41 and SBA-15), have attracted extensive attention due to their properties such as a large surface area and ease of surface modification with basic metal oxides.<sup>35–41</sup> The ordered mesoporous silica supported catalysts have always exhibited better catalytic activities than the amorphous silica; however, the ordered mesoporous structures are not stable at high temperatures in the presence of water produced by reverse water gas

shift reaction.<sup>40</sup> Therefore, it is preferred to use amorphous silica as the catalyst support, which is commercialized for bulk production and far cheaper than ordered mesoporous silica.

Zhu *et al.* investigated Mg-promoted Ni/SiO<sub>2</sub> catalysts with different Mg precursors and prepared by different impregnation sequences to be used in CO<sub>2</sub> reforming of methane.<sup>42</sup> The impregnation of Mg(CH<sub>3</sub>COO)<sub>2</sub> prior to Ni led to the stronger interaction of nickel species with the support and the formation of stable Ni<sub>2</sub>SiO<sub>4</sub> and Mg<sub>2</sub>SiO<sub>4</sub> species, which inhibited the sintering of metallic Ni and resulted in better activity and stability of the catalyst. No significant carbon deposition was observed on the surface of the catalysts, keeping the catalyst stable.<sup>42</sup> Liu's group reported that the Ga<sub>2</sub>O<sub>3</sub> doped Ni/SiO<sub>2</sub> catalyst showed high activity and stability as the presence of Ga<sub>2</sub>O<sub>3</sub> enhanced CO<sub>2</sub> adsorption.<sup>43</sup> Zhu *et al.* compared the promoting effects of La, Mg, Co and Zn on the catalytic properties of the Ni/SiO<sub>2</sub> catalyst for dry CO<sub>2</sub> reforming of CH<sub>4</sub>.<sup>44</sup> They found that both Ni–La/SiO<sub>2</sub> catalysts exhibited greater stability than the other doped catalysts due to the addition of rare earth metals which resulted in a higher degree of dispersion of NiO particles on the catalyst support surface with reduced carbon deposition due to enhanced interactions between Ni and the SiO<sub>2</sub> support.<sup>42</sup> The beneficial effect of La<sub>2</sub>O<sub>3</sub> addition can be attributed to its introduction of basic sites enhancing CO<sub>2</sub> adsorption on the catalyst to form La<sub>2</sub>O<sub>2</sub>CO<sub>3</sub> which removes the carbon on the catalyst *via* the following reaction: La<sub>2</sub>O<sub>2</sub>CO<sub>3</sub> + C → La<sub>2</sub>O<sub>3</sub> + 2CO.<sup>45</sup> Other than suppressing carbon deposition, La<sub>2</sub>O<sub>3</sub> was also reported to prevent metal sintering. La<sub>2</sub>O<sub>3</sub> added as a promoter to a Ni/SiO<sub>2</sub> catalyst is able to interact strongly with the Ni metal, thereby promoting high dispersion of Ni particles over the catalyst surface and reducing the Ni particle size.<sup>34</sup>

Besides doping with different metal oxides to improve the basicity of the Ni/SiO<sub>2</sub> catalyst, a lot of research studies have been done to improve nickel dispersion on silica, which is an effective method to enhance the Ni/SiO<sub>2</sub> catalyst's activity and stability. Zheng's group reported that the Ni/SiO<sub>2</sub> catalysts prepared with nickel citrate displayed high activities and stabilities because of their high nickel dispersion on the support and strong interaction between nickel and the support.<sup>46,47</sup> Lately, a highly dispersed Ni/SiO<sub>2</sub> was achieved by impregnating nickel nitrate on SiO<sub>2</sub> modified with ethylene glycol, which significantly changed the surface properties of the silica support and showed good activity with less carbon deposition toward DRM.<sup>48</sup> Liu's group utilized plasma to treat the Ni/SiO<sub>2</sub> catalyst, and the resistance of the Ni/SiO<sub>2</sub> catalyst to coking was significantly enhanced owing to the stronger metal–support interaction and higher nickel dispersion.<sup>49</sup> Interestingly, de Jong's group reported the preparation of highly dispersed nickel on SBA-15 by nitric oxide controlled thermal decomposition of nitrates.<sup>50</sup> Most recently, nickel–silicide colloids [Ni<sub>x</sub>Si–C<sub>8</sub>H<sub>17</sub>], which are formed by reacting Ni(1,5-cyclooctadiene)<sub>2</sub> with octylsilane in the presence of H<sub>2</sub>, have been used as a precursor to prepare highly dispersed supported nickel catalysts, which exhibit good catalytic activity and stability for DRM.<sup>51</sup> Although numerous researches have been carried out to improve the

activities and stabilities on Ni/SiO<sub>2</sub>, however, carbon deposition is still an unresolved problem without compromise with activities and stabilities using a simple preparation method and cheap nickel precursors.

To improve nickel dispersion is one of the important underlying principles to design an anti-coking catalyst. If the Ni particle size is less than several nanometers during the reforming reactions, the coke formation will be totally inhibited.<sup>52</sup> However, it is a challenge to achieve a highly active and stable catalyst owing to its poor nickel dispersion on a silica support. Previously, we reported that a highly dispersed Ni/SiO<sub>2</sub> catalyst (particle size: <3.0 nm) prepared by an *in situ* self-assembled core-shell precursor route, wherein it would *in situ* self-assemble to form a core-shell (nickel nitrate species as the core and nickel oleate as the shell) precursor as oleic acid is added to the impregnated solution, showed good catalytic activity and stability at 700 °C with negligible carbon deposition after 100 hours of reaction on stream.<sup>53</sup> However, the methane conversion slightly decreased from ~70% to ~60% after 100 hours of reaction at a high space velocity. Therefore, improvements can still be made to the catalytic activity and stability. Herein, we would like to design a supported nickel catalyst by increasing its basicity and nickel dispersion on silica in order to achieve an anti-coking catalyst for DRM reaction. From the literature knowledge mentioned above, La<sub>2</sub>O<sub>3</sub> should be a good dopant for DRM reaction. Therefore, highly dispersed Ni/SiO<sub>2</sub> catalysts doped with La<sub>2</sub>O<sub>3</sub> via an *in situ* self-assembled core-shell precursor route are reported.

## Experimental

### Catalyst preparation

The silica support (silica gel 60, 20–50 μm particle size, specific surface area: 753 m<sup>2</sup> g<sup>-1</sup>, mean pore size = 7.5 nm) was provided by Kanto Chemicals Co. Inc. The metal nitrates of AR purity were bought from Sigma-Aldrich and used directly without further purification. The catalyst preparation procedure followed our previous method.<sup>53</sup> The preparation process is described as follows. 5 wt% Ni/SiO<sub>2</sub> was doped with 1 wt% La<sub>2</sub>O<sub>3</sub> by incipient wetness impregnation. This preparation method involved the initial solvation of Ni and lanthanum nitrate hexahydrate in water to form a mixed salt solution, then a desired amount of oleic acid (OA) at a molar ratio of OA/(Ni + La) = 0.5 was added to the solution. Firstly, 1.32 g of nickel nitrate hexahydrate and 0.14 g of lanthanum nitrate hexahydrate (from Sigma-Aldrich) were dissolved in 9 mL of D.I. water, and then 0.68 g of oleic acid (from Sigma-Aldrich) was added into the solution. Finally, 5 g of spherical silica was introduced into the above solution. The impregnated catalysts were aged at room temperature for more than 6 hours before the catalysts were dried at 100 °C overnight. Finally the catalysts were calcined at 700 °C for 4 hours. The 5 wt% Ni–1 wt% La<sub>2</sub>O<sub>3</sub>/SiO<sub>2</sub> (5% Ni/SiO<sub>2</sub>) catalysts prepared with OA and without OA were designated as NiLaSi–OA (NiSi–OA) and NiLaSi (NiSi), respectively.

### Powder X-ray diffraction (XRD)

XRD analysis was conducted using a Shimadzu LabX XRD-6000 X-ray diffractometer with Cu K<sub>α</sub> radiation (wavelength, λ = 0.154056 nm) and operated at a current of 30 mA and a voltage of 40 kV. NiO or Ni crystallite sizes were calculated using the Scherrer equation. In order to estimate the average Ni crystallite size on the reduced catalysts, prior to XRD analysis, the fresh catalysts were reduced in a H<sub>2</sub> atmosphere (purity = 99.99%) at 700 °C for 1 hour at a H<sub>2</sub> gas flow rate of 10 ml min<sup>-1</sup>. Subsequently, the reduced catalysts were cooled down from 700 °C to room temperature under an H<sub>2</sub> atmosphere. Then the reduced catalysts were transferred quickly to an XRD chamber to perform XRD measurement.

### Hydrogen temperature-programmed reduction (H<sub>2</sub>-TPR)

The reduction behavior of the prepared fresh catalysts was analyzed using H<sub>2</sub>-TPR. H<sub>2</sub>-TPR tests were carried out using a ChemBET-3000 TPR/TPD. 0.05 g of the catalyst was loaded into a quartz U-tube (I.D. 1/4 inch) and heated in a furnace at a H<sub>2</sub>-N<sub>2</sub> mixture (5 wt% H<sub>2</sub>, balance N<sub>2</sub>) gas flow rate of 30 ml min<sup>-1</sup> and a linear heating rate of 10 °C min<sup>-1</sup>. The signal from H<sub>2</sub> consumption was detected by a TCD detector and recorded on a PC.

### Differential thermal analysis and thermal gravimetry analysis (DTA-TGA)

DTA-TGA was carried out using a Shimadzu DTG-60 thermo-analyzer. Approximately 8 mg of the catalyst sample was heated in an atmosphere of air from room temperature to 800 °C at a heating rate of 10 °C min<sup>-1</sup>.

### Transmission electron microscopy (TEM)

TEM images were taken using a JEOL JEM-2100F. Prior to TEM analysis, the catalysts were reduced at 700 °C in purified H<sub>2</sub> for one hour. The samples were dispersed in ethanol solution and ultrasonicated for 30 min. Then, the above solutions were dropped onto the copper grid for TEM observation.

### Catalytic activity tests

The DRM reactions were carried out in a quartz reactor (I.D. = 1/4 inch). The catalyst under study was loaded and packed in the middle of the quartz tube using quartz wool which is inert in the reaction. Under atmospheric pressure, the catalyst was heated from the initial room temperature to a reaction temperature of 700 °C at a rate of 20.0 °C min<sup>-1</sup>. Reactions at a total flow rate of 60 ml min<sup>-1</sup> of a feed gas with a molar ratio of CH<sub>4</sub>/CO<sub>2</sub>/N<sub>2</sub> = 1/1/1 were carried out. Prior to the catalytic reaction, 0.05 g or 0.005 g of the catalyst was reduced in a H<sub>2</sub> atmosphere at 700 °C for 1 hour. A cold trap was employed to remove any water from the effluent gas stream prior to gas analysis using an on-line gas chromatograph (GC). Effluent gas from the reactor was analyzed using an Agilent GC equipped with 5A molecular sieve and Poropak Q

columns.  $N_2$  was used as the internal standard to calculate the conversions of  $CH_4$  and  $CO_2$ .

## Results and discussion

Fig. 1 depicts XRD patterns of NiLaSi and NiLaSi-OA. Sharp NiO phase peaks on the NiLaSi catalyst could be seen clearly. However, the NiO peaks were almost invisible on the NiLaSi-OA catalyst, indicating that NiO was highly dispersed on the support. The crystalline size of NiO on the NiLaSi catalyst was 8.7 nm as estimated by the Scherrer equation. The nickel crystalline sizes on reduced NiLaSi, NiSi-OA and NiLaSi-OA catalysts are 10.6, 2.9 and 3.0 nm, respectively. Although the Ni crystalline sizes on NiSi-OA and NiLaSi-OA catalysts were almost the same, the diffraction peak area of nickel on NiSi-OA was significantly bigger than that on NiLaSi-OA (shown in Fig. 1S<sup>†</sup>), which suggests that the number of detectable nickel crystallines on the reduced NiSi-OA was higher than those on the reduced NiLaSi-OA, *i.e.* the nickel crystalline size on reduced NiLaSi-OA is smaller than that on reduced NiSi-OA.

### H<sub>2</sub>-TPR results

H<sub>2</sub>-TPR is a useful technique to characterize the reduction properties of a catalyst for correlation with its catalytic performance. Fig. 2 shows the H<sub>2</sub>-TPR curves of NiLaSi and NiLaSi-OA catalysts. The position of peaks from H<sub>2</sub>-TPR on NiLaSi catalyst was almost the same with those on NiSi that the NiO showed weak interaction with the silica support, which could be reduced at low temperature (<500 °C).<sup>53</sup> However, the reduction peak of the NiSi-OA catalyst was at 609 °C,<sup>53</sup> but the NiLaSi-OA catalyst showed a high reduction peak at 640 °C, indicating that a more stable nickel silicate species was formed because of the addition of La<sub>2</sub>O<sub>3</sub>.

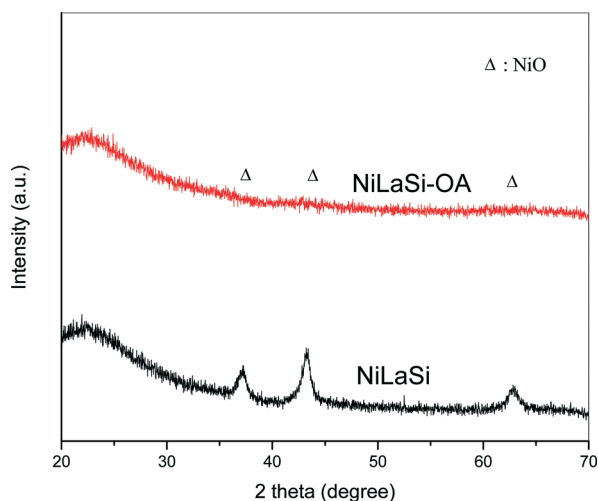


Fig. 1 XRD patterns of NiLaSi and NiLaSi-OA.

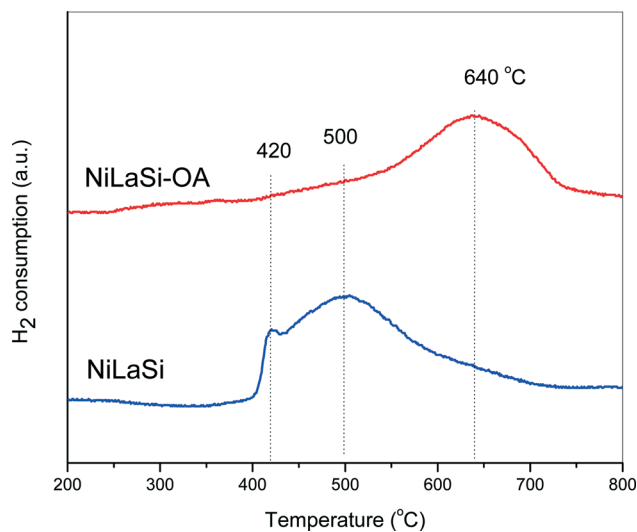


Fig. 2 TPR profiles of NiLaSi and NiLaSi-OA.

## TEM results

Fig. 3(A) displays the TEM image of the reduced NiLaSi catalyst. Big particles could be observed clearly. The La<sub>2</sub>O<sub>3</sub> phase could not be detected in the XRD pattern (Fig. 1) since it was highly dispersed on the support. Furthermore, the La<sub>2</sub>O<sub>3</sub> loading was as low as 1 wt.% and hence it could not distribute densely on the support. Therefore, particles observed in the TEM image should be primarily nickel particles. The mean particle size of nickel was 15.5 nm on the reduced NiLaSi catalyst, which was bigger than the crystalline size (10.6 nm) measured by XRD. However, nickel particles with a size <2.0 nm were homogeneously dispersed on the NiLaSi-OA catalyst (Fig. 3(B)). The mean nickel particle size on NiSi-OA observed using STEM was 2.9 nm.<sup>53</sup> The TEM results hence showed that OA can effectively promote the dispersion of nickel. Furthermore, it was previously shown by XRD that the addition of lanthanum oxide further promoted the dispersion of nickel.

### Catalytic activities

The catalytic activities of NiLaSi and NiLaSi-OA were tested at 700 °C with GHSV = 72 000 ml g<sup>-1</sup> (cat) h<sup>-1</sup>. The NiLaSi catalyst showed poor catalytic activities and such severe carbon formation that the catalyst bed was blocked in one hour of reaction on stream. The initial CH<sub>4</sub> and CO<sub>2</sub> conversions over the NiLaSi catalyst were 69.8% and 79.0%, respectively. Surprisingly, the NiLaSi-OA catalyst not only showed high catalytic activity but also high stability as shown in Fig. 4. The conversions of CH<sub>4</sub> and CO<sub>2</sub> were ~80% and ~85% during reaction for 100 hours of reaction on stream. The H<sub>2</sub>/CO product molar ratio was also maintained at around 0.85. In contrast, the NiSi-OA without the promoter La<sub>2</sub>O<sub>3</sub> showed lower catalytic activity and stability.<sup>53</sup> In order to further investigate the stability of the NiLaSi-OA catalyst, a high GHSV (720 000 ml g<sup>-1</sup> (cat) h<sup>-1</sup>) was used to make sure that

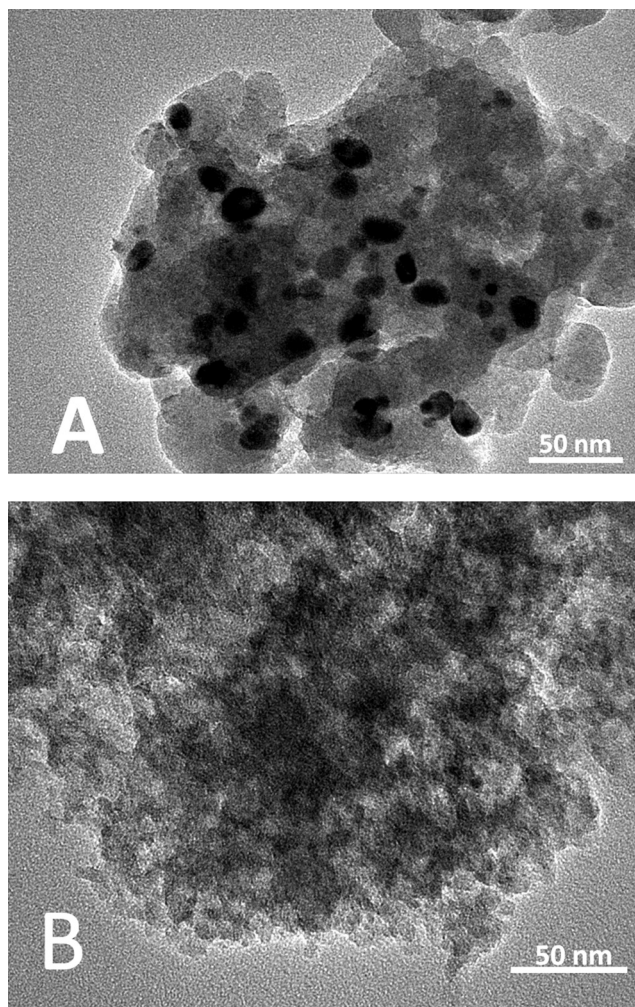


Fig. 3 TEM images of NiLaSi (A) and NiLaSi-OA (B) catalysts.

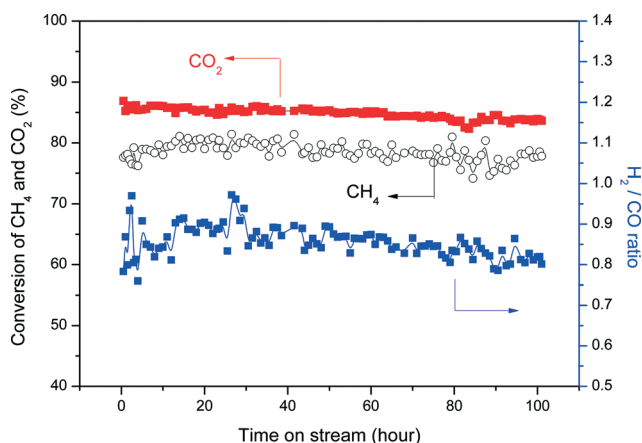


Fig. 4 Catalytic performance of NiLaSi-OA for DRM reaction at 700 °C with GHSV = 72 000 ml g<sup>-1</sup> (cat) h<sup>-1</sup> (0.05 g catalyst,  $F_{\text{CH}_4} = F_{\text{CO}_2} = F_{\text{N}_2} = 60$  ml min<sup>-1</sup>).

the conversions were lower than the thermodynamic equilibrium value as shown in Fig. 5. The conversions of CH<sub>4</sub> and CO<sub>2</sub> dropped slightly around 7% after 100 hours of reaction

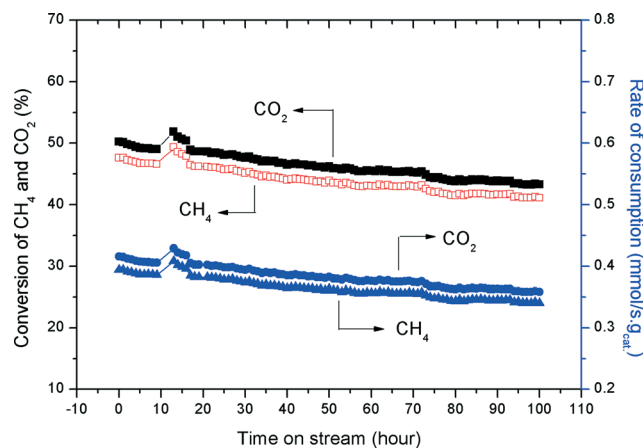


Fig. 5 Catalytic performance of NiLaSi-OA for DRM reaction at 700 °C with GHSV = 720 000 ml g<sup>-1</sup> (cat) h<sup>-1</sup> (0.005 g catalyst,  $F_{\text{CH}_4} = F_{\text{CO}_2} = F_{\text{N}_2} = 60$  ml min<sup>-1</sup>).

on stream. The consumption rates of CH<sub>4</sub> and CO<sub>2</sub> were also calculated. The initial consumption rates of CH<sub>4</sub> and CO<sub>2</sub> were 0.41 and 0.39 mmol s<sup>-1</sup> g<sup>-1</sup> (cat), which decreased to 0.36 and 0.34 mmol s<sup>-1</sup> g<sup>-1</sup> (cat) after 100 hours of reaction on stream.

#### Characterization of spent catalysts

Fig. 6 shows the XRD patterns of spent NiLaSi and NiLaSi-OA catalysts. The spent NiLaSi catalyst showed an evident peak at  $2\theta = 26^\circ$ , which was assigned to graphite.<sup>47</sup> The crystalline size of nickel on the spent NiLaSi catalyst was 12.3 nm, which was almost the same as that on the freshly reduced catalyst. However, the spent NiLaSi-OA catalyst had no graphite peak. The nickel crystalline size on the spent NiLaSi-OA catalyst was 5.5 nm, which slightly increased compared to that on the freshly reduced catalyst (3.0 nm).

Fig. 7 displays TEM images of spent NiLaSi and NiLaSi-OA catalysts. From the TEM image of the spent NiLaSi catalyst

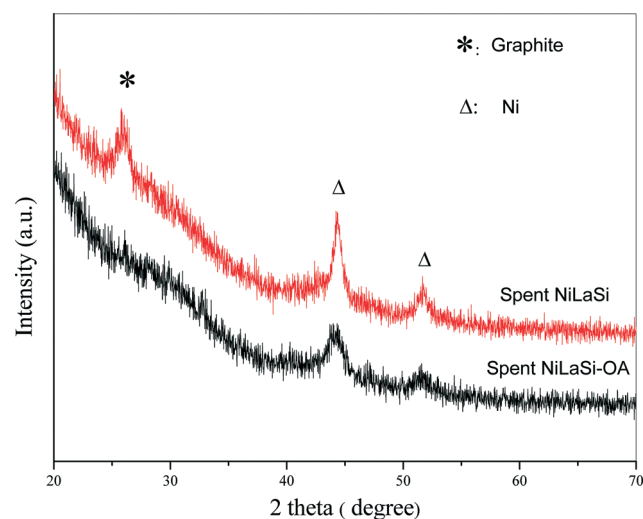


Fig. 6 XRD patterns of spent NiLaSi and NiLaSi-OA catalysts.

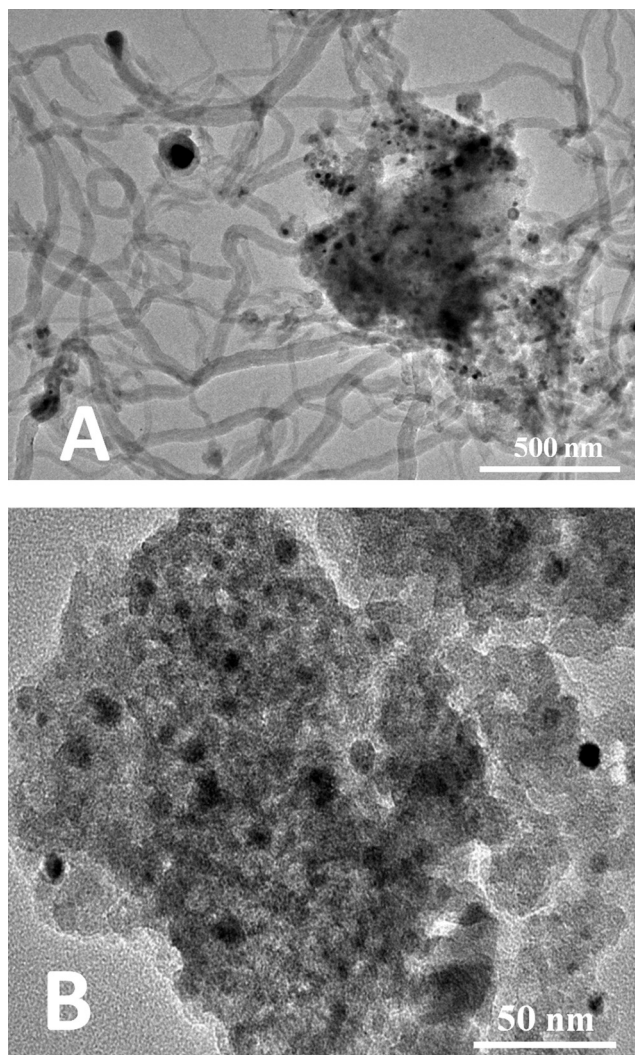


Fig. 7 TEM images of spent NiLaSi (A) and NiLaSi-OA (B) catalysts.

(Fig. 7A), a lot of carbon nanotubes are observed. However, no carbon nanotube on the spent NiLaSi-OA catalyst is found, although a few nickel particles were sintered to around 9.0 nm as shown by the particle marked with a red circle (Fig. 7B). The TEM results are further confirmed by DTA-TGA results (Fig. 8).

Fig. 8(A) shows the DTA-TGA curves of the spent NiLaSi catalyst. The DTA curve shows two group peaks: one is a negative peak (endothermic peak) and the other one is positive (exothermic peak). The negative peak centered at 57 °C is assigned to the desorption of physical water. The two overlapping positive peaks at 611 °C and 645 °C are ascribed to the carbon species combustion. The two overlapping positive peaks mean that there are two kinds of carbon species on the spent catalyst. Based on the weight loss in the TGA curve, the sample amount after carbon was removed and the reaction time on stream, the carbon formation rate on the NiLaSi catalyst is as high as 146.2 mg (carbon) g<sup>-1</sup> (cat) h<sup>-1</sup>. Interestingly, the spent NiLaSi-OA catalyst did not show any exothermic peak in the DTA curve at high temperature.

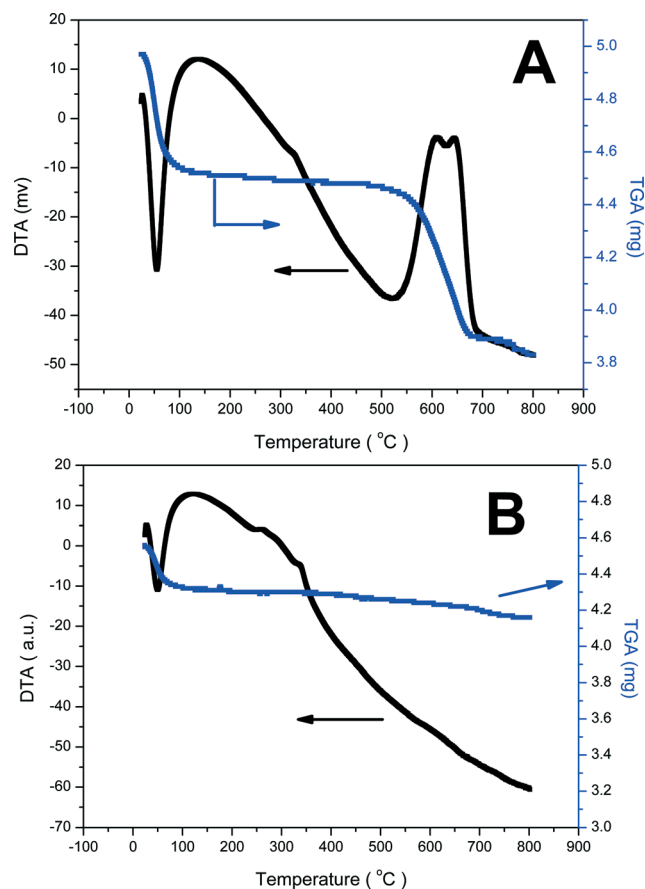


Fig. 8 DTA-TGA curves of spent NiLaSi (A) and NiLaSi-OA (B) catalysts.

However, weak exothermic peaks could be observed between 260 and 350 °C; these weak peaks are attributed to the oxidation of metal nickel on the spent NiLaSi-OA catalyst. Some weight loss is observed in the TGA curve between 300 and 800 °C. In order to exclude the possibility that the weight loss was caused by carbon combustion, a pure silica support was used in the DTA-TGA experiment. Fig. 2S† clearly shows that the TGA curve of silica is similar to that of the spent NiLaSi-OA catalyst. Therefore, these results show that no carbon is formed on the spent NiLaSi-OA catalyst.

It is well known that physical adsorption of CO<sub>2</sub> can only occur on a silica support at low temperature <100 °C.<sup>34,43</sup> CO<sub>2</sub> activation is a key step for DRM reaction to remove the carbon deposit due to CH<sub>4</sub> decomposition, which is the main source of active carbon.<sup>49,54,55</sup> If the adsorbed (activated) CO<sub>2</sub> reacted too slowly with the active carbon on the catalyst surface, the active carbon would precipitate and polymerize to form inert graphite.<sup>43</sup> Therefore, the addition of La<sub>2</sub>O<sub>3</sub> promotes the adsorption of CO<sub>2</sub>, facilitating carbon removal on the nickel particles. Furthermore, it is widely accepted that the particle size of nickel and the interaction between metal and the support are critical factors that affect carbon deposition on a catalyst.<sup>34,42,43,46,47,49,52</sup> From XRD, TPR and TEM results, the addition of La<sub>2</sub>O<sub>3</sub> promoted the dispersion of nickel and enhanced the interaction between nickel and the

support. As a consequence, the NiLaSi-OA catalyst showed excellent activity and stability during 100 hours of reaction on stream with negligible carbon deposition. In comparison, the NiSi-OA catalyst was able to withstand 100 hours of reaction with negligible carbon deposition, but exhibited lower activity levels.

## Conclusions

The highly dispersed and anti-coking NiLaSi-OA catalyst ( $d_{\text{Ni}} < 3.0$  nm) was successfully prepared *via* an *in situ* self-assembled core-shell precursor route.  $\text{La}_2\text{O}_3$  promoted the dispersion of nickel and enhanced the interaction between nickel oxide and the support. The NiLaSi-OA catalyst exhibited excellent catalytic activity and stability without coke formation after 100 hours of reaction on stream for syngas production by DRM. The strategy reported in this paper can be potentially extended to prepare other highly dispersed supported metal catalysts.

## Acknowledgements

The authors gratefully thank the National University of Singapore and A\*STAR (A\*STAR SERC grant no. 092-138-0022, RP no. 279-000-292-305), the NEA (NEA-ETRP grant no.1002114, RP no. 279-000-333-490), and the NRF (NRF-POC 001-055) for generously supporting this work. L.Y. Mo sincerely thanks Y. Kathiraser, Z.W. Li, E.T. Saw and M.L. Ang for their beneficial discussion and help in the experiments.

## Notes and references

- M. C. J. Bradford and M. A. Vannice, *Catal. Rev.: Sci. Eng.*, 1999, **41**, 1.
- C. H. Bartholomew, *Catal. Rev.: Sci. Eng.*, 1982, **24**, 67.
- D. L. Trimm, *Catal. Rev.: Sci. Eng.*, 1977, **16**, 155.
- J. T. Richardson and S. A. Paripatyadar, *Appl. Catal., A*, 1990, **61**, 293.
- P. D. F. Vernon, M. L. H. Green, A. K. Cheetham and A. T. Ashcroft, *Catal. Today*, 1992, **13**, 417.
- J. R. Rostrup-Nielsen and J. H. Bak-Hansen, *J. Catal.*, 1993, **144**, 38.
- J. H. Edwards and A. M. Maitra, *Fuel Process. Technol.*, 1995, **42**, 269.
- K. Tomishige, Y. G. Chen and K. Fujimoto, *J. Catal.*, 1999, **181**, 91.
- J. R. Rostrup-Nielsen and J. H. B. Hansen, *J. Catal.*, 1993, **144**, 38.
- S. Wang and G. Q. Lu, *Appl. Catal., B*, 1998, **16**, 269.
- H. Y. Wang and E. Ruckenstein, *Appl. Catal., A*, 2000, **204**, 143.
- Z. L. Zhang and X. E. Verykios, *Appl. Catal., A*, 1996, **138**, 109.
- Z. L. Zhang, X. E. Verykios, S. M. MacDonald and S. Affrossman, *J. Phys. Chem.*, 1996, **100**, 744.
- K. Sutthiumporn and S. Kawi, *Int. J. Hydrogen Energy*, 2011, **36**, 14435.
- Y. Kathiraser, W. Thitsartarn, K. Sutthiumporn and S. Kawi, *J. Phys. Chem. C*, 2013, **117**, 8120.
- J. Ni, L. Chen, J. Lin and S. Kawi, *Nano Energy*, 2012, **1**, 674.
- B. Q. Xu, J. M. Wei, Y. T. Yu, Y. Li, J. L. Li and Q. M. Zhu, *J. Phys. Chem. B*, 2003, **107**, 5203.
- J. J. Guo, H. Lou, H. Zhao, D. F. Chai and X. M. Zheng, *Appl. Catal., A*, 2004, **273**, 75.
- J. Ni, L. Chen, J. Lin, M. K. Schreyer, Z. Wang and S. Kawi, *Int. J. Hydrogen Energy*, 2013, **38**, 13631.
- Y. G. Chen, K. Tomishige, K. Yokoyama and K. Fujimoto, *J. Catal.*, 1999, **184**, 479.
- K. Tomishige, Y. G. Chen and K. Fujimoto, *J. Catal.*, 1999, **181**, 91.
- Y. H. Hu and E. Ruckenstein, *Catal. Lett.*, 1996, **36**, 145.
- Y. G. Chen, K. Tomishige, K. Yokoyama and K. Fujimoto, *Appl. Catal., A*, 1997, **165**, 335.
- Y. G. Chen, O. Yamazaki, K. Tomishige and K. Fujimoto, *Catal. Lett.*, 1996, **39**, 91.
- J. G. Zhang, H. Wang and A. K. Dalai, *J. Catal.*, 2007, **249**, 300.
- J. J. Guo, H. Lou, Y. H. Zhu and X. M. Zheng, *Mater. Lett.*, 2003, **57**, 4450.
- R. Pereñíguez, V. M. Gonzalez-delaCruz, A. Caballero and J. P. Holgado, *Appl. Catal., B*, 2012, **123**, 324.
- R. Pereñíguez, V. M. Gonzalez-delaCruz, J. P. Holgado and A. Caballero, *Appl. Catal., B*, 2010, **93**, 346.
- K. Sutthiumporn, T. Maneerung, Y. Kathiraser and S. Kawi, *Int. J. Hydrogen Energy*, 2012, **37**, 11195.
- M. C. J. Bradford and A. M. Vannice, *Appl. Catal., A*, 1996, **142**, 73.
- S. Wang and G. Q. Lu, *Appl. Catal., B*, 1998, **16**, 269.
- V. C. H. Kroll, H. M. Swaan and C. Mirodatos, *J. Catal.*, 1996, **161**, 409.
- F. Pompeo, N. N. Nichio, M. G. Gonzalez and M. Montes, *Catal. Today*, 2006, **107-108**, 856.
- L. Y. Mo, X. M. Zheng, Q. S. Jing, H. Lou and J. H. Fei, *Energy Fuels*, 2005, **19**, 49.
- D. Liu, R. Lau, A. Borgna and Y. Yang, *Appl. Catal., A*, 2009, **358**, 110.
- D. Liu, X. Y. Quek, H. H. A. Wah, G. Zeng, Y. Li and Y. Yang, *Catal. Today*, 2009, **148**, 243.
- S. Yasyerli, S. Filizgok, H. Arbag, N. Yasyerli and G. Dogu, *Int. J. Hydrogen Energy*, 2011, **36**, 4863.
- N. Wang, X. Yu, K. Shen, W. Chu and W. Qian, *Int. J. Hydrogen Energy*, 2013, **38**, 9718.
- S. Damyanova, B. Pawelec, K. Arishtirova, J. L. G. Fierro, C. Sener and T. Dogu, *Appl. Catal., B*, 2009, **92**, 250.
- H. Liu, Y. Li, H. Wu, H. Takayama, T. Miyake and D. He, *Catal. Commun.*, 2012, **28**, 168.
- N. Wang, K. Shen, X. P. Yu, W. Z. Qian and W. Chu, *Catal. Sci. Technol.*, 2013, **3**, 2278.
- J. Q. Zhu, X. X. Peng, L. Yao, D. M. Tong and C. W. Hu, *Catal. Sci. Technol.*, 2012, **2**, 529.
- Y. X. Pan, P. Y. Kuai, Y. Liu, Q. F. Ge and C. J. Liu, *Energy Environ. Sci.*, 2010, **3**, 1322.
- J. Q. Zhu, X. X. Peng, L. Yao, J. Shen, D. M. Tong and C. W. Hu, *Int. J. Hydrogen Energy*, 2011, **36**, 7094.

- 45 V. A. Tsipouriari and X. E. Verykios, *J. Catal.*, 1999, **187**, 85.
- 46 S. F. He, H. M. Wu, W. J. Yu, L. Y. Mo, H. Lou and X. M. Zheng, *Int. J. Hydrogen Energy*, 2009, **34**, 839.
- 47 S. F. He, Q. S. Jing, W. J. Yu, L. Y. Mo, H. Lou and X. M. Zheng, *Catal. Today*, 2009, **148**, 137.
- 48 X. Y. Lv, J. F. Chen, Y. S. Tan and Y. Zhang, *Catal. Commun.*, 2012, **20**, 6.
- 49 Y. X. Pan, C. J. Liu and P. Shi, *J. Power Sources*, 2008, **176**, 46.
- 50 J. R. A. Sietsma, J. D. Meeldijk, J. P. den Breejen, M. Versluijs-Helder, A. J. van Dillen, P. E. de Jongh and K. P. de Jong, *Angew. Chem., Int. Ed.*, 2007, **46**, 4547–4549.
- 51 D. Baudouin, K. C. Szeto, P. Laurent, A. D. Mallmann, B. Fenet, L. Veyre, U. Rodemerck, C. Coperet and C. Thieuleux, *J. Am. Chem. Soc.*, 2012, **134**, 20624.
- 52 C. J. Liu, J. Y. Ye, J. J. Jiang and Y. X. Pan, *ChemCatChem*, 2011, **3**, 529.
- 53 L. Y. Mo, E. T. Saw, Y. H. Du, A. Borgna, M. L. Ang, Y. Kathiraser, Z. W. Li, W. Thitsartarn, M. Lin and S. Kawi, unpublished results.
- 54 Z. Xu, Y. M. Li, J. Y. Zhang, L. Chang, R. Q. Zhou and Z. T. Duan, *Appl. Catal., A*, 2001, **210**, 45.
- 55 S. B. Wang and G. Q. M. Lu, *Energy Fuels*, 1998, **12**, 248.